Exploring the impact of Cordilleran Ice Sheet size on marine-terminating ice stream grounding line dynamics

T. Pico [a],[*] , S. Kodama [a], C. Vigilia [b], A. Robel [c]

[a] *Earth and Planetary Science, University of California Santa Cruz, Santa Cruz, CA, USA*
[b] *Jackson School of Geosciences, University of Texas at Austin, Austin, TX, USA*
[c] *School of Earth and Atmospheric Sciences, Georgia Institute of Technology, Atlanta, GA, USA*

ARTICLE INFO

ABSTRACT

The growth and retreat of the Cordilleran Ice Sheet prior to the Last Glacial Maximum, during Marine Isotope Stage 3 (MIS 3; 57 ka to 29 ka), is elusive. Yet ice sheet size impacts underlying topography through glacial isostatic adjustment, which can modulate ice stream grounding zone dynamics. In this study, we explore bounds on MIS 3 Cordilleran Ice Sheet volume, and predict how topographic change due to glacial isostatic adjustment would shift the zones where grounding lines can persist for key Cordilleran ice streams. We identified three key ice streams (Yakutat Sea Valley, Skeena Valley, Juan de Fuca Strait), two of which are located near sites with sediment cores recording active ice dynamics across this time interval. We used the reconstructed bedrock topography for these ice streams to assess how glacial isostatic adjustment would change the potential zones of grounding line persistence, based on plausible end-member Cordilleran Ice Sheet histories. We found that glacial isostatic adjustment shifts the locations of persistent grounding line zones differently, based on the location of the Cordilleran ice stream with respect to the predicted spatial pattern of topographic change. Depending on the size of the Cordilleran Ice Sheet in the period leading into the Last Glacial Maximum, glacial isostatic adjustment could have acted to either stabilize or destabilize marine-terminating grounding lines across the Pacific shelf. Future work refining the Cordilleran Ice Sheet history across the glacial build-up phase will disentangle the role of solid Earth feedbacks on grounding line dynamics for individual ice streams, and provide insight into the mechanisms causing abrupt climate events, ranging from rapid ice discharge to megafloods, documented in the North Pacific across the last ice age.

1. Introduction

The Cordilleran Ice Sheet spanned the Rocky Mountains and merged with the Laurentide Ice Sheet during the Last Glacial Maximum (26 ka; LGM; Marine Isotope Stage (MIS) 2; Clark et al., 2009). The history of this former continental ice sheet is challenging to reconstruct due to relatively sparse field observations within its mountainous terrain (Clague and James, 2002; Booth et al., 2003; Clague et al., 2005; Stroeven et al., 2010; Seguinot et al., 2016; Eyles et al., 2018). Prior to the Last Glacial Maximum, records of Cordilleran Ice Sheet size and extent are even more rare, as ice sheets destroy prior evidence of their margins as they advance (Stokes et al., 2015). Indeed, land-based observational constraints on Cordilleran ice extent across the glaciation phase during MIS (Marine Isotope Stage) 3 (57 - 29 ka; Lisiecki and Raymo, 2005) are limited (Batchelor et al., 2019; Dalton et al., 2022a,b). The terrestrial record suggests an extensive ice margin near 55 ka, followed by an unconstrained degree of ice sheet retreat before growing to MIS 2 maximum extent (Clague et al., 1990; Clague et al., 2005; Ward et al., 2007; Briner and Kaufman, 2008; Stroeven et al., 2010, 2014, p. 201; Kaufman et al., 2011; McDonald et al., 2012; Lesemann et al., 2013; Mathewes et al., 2015; Hebda et al., 2016). Complementing this land-based evidence is the marine geologic record, which indicates active ice dynamics along the Pacific sector of the Cordilleran Ice Sheet across this interval (Hewitt et al., 1997; Cosma and Hendy, 2008; Hendy and Cosma, 2008; Maier et al., 2018; Walczak, 2020a,b).

The behavior of marine terminating ice streams, whose dynamics can be recorded in sedimentary cores, are highly sensitive to underlying topography and bed slopes (Schoof, 2007, 2012; Robel et al., 2018). Grounding lines spend long periods of time on topographic highs, where reduced ice flow velocities slow ice margin retreat (Alley, 1993; Favier

et al., 2016; Robel et al., 2022; McKenzie et al., 2023). Over the ice age, the topography that underlies marine terminating ice streams is modulated by glacial isostatic adjustment (GIA), or the solid Earth's response to the loading and unloading of ice sheets, and this process has been shown to impact grounding line retreat rates (Gomez et al., 2010; Adhikari et al., 2014; Kingslake et al., 2018). The size and duration of ice loading impacts the magnitude of topographic change, which can shift bedrock elevations and zones where grounding lines tend to persist. The feedback between ice sheet size, glacial isostatic adjustment-induced topography change, and grounding line migration is important for characterizing the behavior of ice streams today in places like Antarctica (Gomez et al., 2010; Adhikari et al., 2014; Barletta et al., 2018), and may be useful for elucidating ice sheet behavior in the past (Kingslake et al., 2018; Pico et al., 2019; Whitehouse et al., 2019; Kodama et al., 2025). Here, we wish to explore the impact of Cordilleran Ice Sheet size on zones of grounding line persistence during the build-up phase of the last ice age.

Existing reconstructions of Cordilleran Ice Sheet size (thickness and extent) prior to the LGM are based on climate-forced dynamic ice sheet modeling and global ice sheet histories constructed using estimates of ice margins combined with equilibrium ice sheet profiles. Seguinot et al. (2016) performed numerical ice sheet simulations forced with paleo-temperature records from ice core sites in Greenland and Antarctica, and compared their predictions to the sparse set of observables for the Cordilleran Ice Sheet prior to the LGM. Regardless of climate forcing choice, these simulations predicted a large ice sheet between 60 and 55 ka (early MIS 3), similar in size to MIS 2, and a retracted ice sheet between 50 and 40 ka during mid-MIS 3. Another recent reconstruction is based on fitting an equilibrium ice sheet profile to geologic evidence for ice margins, and iteratively adjusting the ice sheet reconstruction to fit a collection of relative sea level data globally (PALEOMIST; Gowan et al., 2021). The PALEOMIST reconstruction includes an extensive Cordilleran Ice Sheet at 55 ka and a near nonexistent ice sheet, constricted to mountain regions, from 47.5 to 35 ka. The PALEOMIST Cordilleran ice history is based on fitting maximum ice margins to mapped moraines

dated to ~55 ka (Clague et al., 1990; Ward et al., 2007; Briner and Kaufman, 2008; Stroeven et al., 2010, 2014, p. 201; McDonald et al., 2012; Lesemann et al., 2013; Mathewes et al., 2015), and assuming extensive retreat in the following time period when there is evidence for high global sea levels (Hebda et al., 2016; Pico et al., 2016; Gowan et al., 2021; Dalton et al., 2022a,b; de Gelder et al., 2022; Farmer et al., 2022; Pico, 2022).

The marine sedimentary record provides an alternate window into Cordilleran Ice Sheet dynamics across the glaciation phase that complements terrestrial glacial and non-glacial deposits constraints on possible ice margins across MIS 3 (Batchelor et al., 2019; Dalton et al., 2019, 2022a,b; Dalton et al., 2022a,b). Ice rafted debris events are recorded in sediment cores in southeastern Alaska margin (termed Siku events; at 41 and 30 ka near Yakutat Sea Valley; Walczak, 2020a,b U1419; YSV; Fig. 1) as well as the British Columbia margin (at 48 ka, 40 ka and 30 ka near Juan de Fuca Strait; Cosma and Hendy, 2008; MD02-2496; JDF; Fig. 1), and the timing of these events across MIS 3 correspond to Heinrich events in the North Atlantic (Hewitt et al., 1997; Hendy and Cosma, 2008; Walczak, 2020a,b). These events suggest active marine terminating ice streams, with ice discharge that carried ice rafted debris. There is also evidence for meltwater events during Heinrich events based on salinity reconstructions in the Gulf of Alaska (Maier et al., 2018).

The cause of these dynamic ice discharge events is unclear. Climate forcings, such as ocean or atmospheric warming, could potentially trigger abrupt ice stream retreat, with ice discharge carrying ice rafted debris (Taylor et al., 2014; Robel and Tziperman, 2016; Bassis et al., 2017; Walczak, 2020a,b). Nevertheless, other mechanisms could play a role in ice dynamics, and in this study we consider the role of changing bedrock topography due to glacial isostatic adjustment on grounding line migration (Gomez et al., 2012; Bassis et al., 2017; Pico et al., 2019; Kodama et al., 2025). Although the size of the Cordilleran Ice Sheet across MIS 3 is largely uncertain, it is possible that the loading history of this ice sheet can exert a feedback on the ice sheet's retreat rate. The Cordilleran Ice Sheet's potential influence on the grounding line
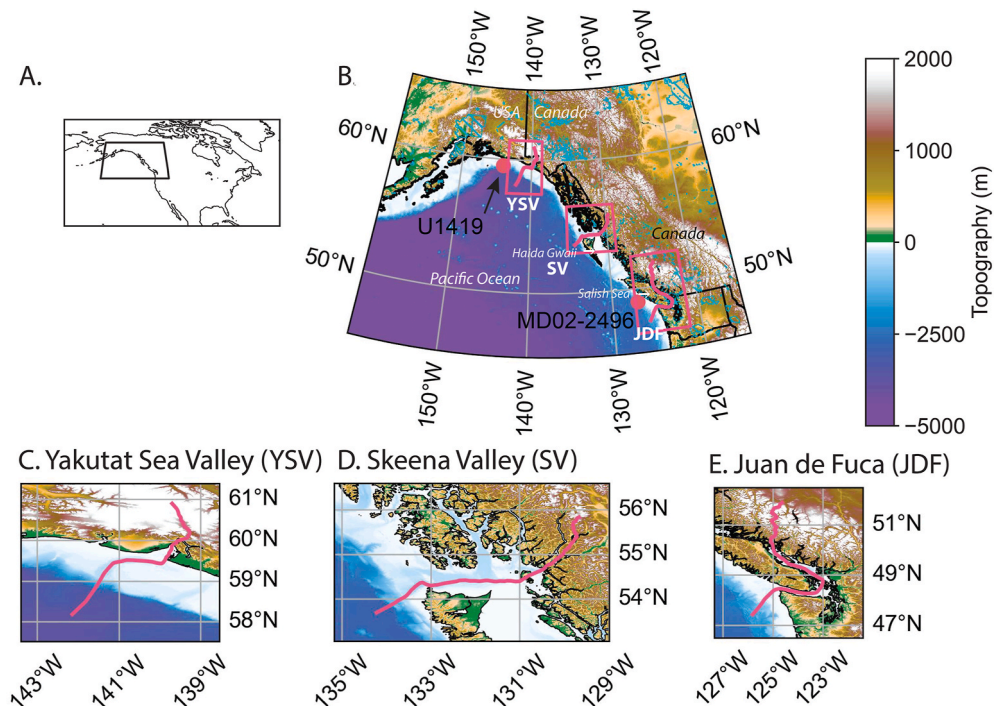

Fig. 1. A. Inset map. B. Present day topography. Red circles show location of sediment cores. Transects of ice streams in magenta for (C) Yakutat Sea Valley (YSV), (D) Skeena Valley (SV), (E) Juan de Fuca Strait (JDF). Teal crosshatches represent Alaska Native Allotments, American Indian Reservations, Indian Reserves, and Yukon First Nations Settlement Lands political boundaries. (For interpretation of the references to colour in this figure legend, the reader is referred to the Web version of this article.)

dynamics of its marine terminating ice streams through ice sheet loading, and subsequent glacial isostatic adjustment-induced topographic change, has not yet been investigated.

We explore constraints on Cordilleran Ice Sheet volume across MIS 3, and predict how glacial isostatic adjustment would change the topography that underlies key ice streams. We identified three key ice streams, including two near locations that record active ice dynamics across this time interval (Yakutat Sea Valley; YSV, and Juan de Fuca Strait; JDF; Fig. 1). We used reconstructed bedrock topography for these ice streams to assess how glacial isostatic adjustment would shift the locations where grounding lines persist based on the range of plausible Cordilleran Ice Sheet histories. While we cannot provide a better constrained MIS 3 Cordilleran Ice Sheet reconstruction, exploration of the possible magnitudes of glacial isostatic adjustment informs our understanding of the role of topographic change on ice stream dynamics. Ultimately, we aim to discover whether glacial isostatic adjustment exerts an important control on the ice dynamics documented in sedimentary records of the North Pacific.

2. Methods

2.1. Glacial isostatic adjustment

The growth and decay of ice sheets over glacial cycles drove a complex spatio-temporal pattern of sea-level change, and equivalently topographic change, due to deformational, gravitational and rotational effects of glacial isostatic adjustment (GIA). Our simulations are based on the sea-level theory and pseudo-spectral algorithm described by Kendall et al. (2005) at a spherical harmonic truncation of degree and order 256. This treatment includes the impact of load-induced Earth rotation changes on sea level (Milne and Mitrovica, 1996), evolving shorelines and the migration of grounded, marine-based ice (Johnston, 1993; Milne et., 1999; Lambeck et al., 2003; Kendall et al., 2005). These predictions require models for Earth's viscoelastic structure and the spatio-temporal history of ice cover. For the Earth structure model, we adopt a mantle viscosity profile based on previous reconstructions for lithospheric thickness and upper mantle viscosity for the Pacific Coast of North America (Clague and James, 2002; James et al., 2009; Yousefi et al., 2018; Clark et al., 2019; Marsman et al., 2021). Specifically, our adopted Earth model is characterized by a lithospheric thickness of 50 km, a low-viscosity zone in the first 200 km of the upper mantle with a
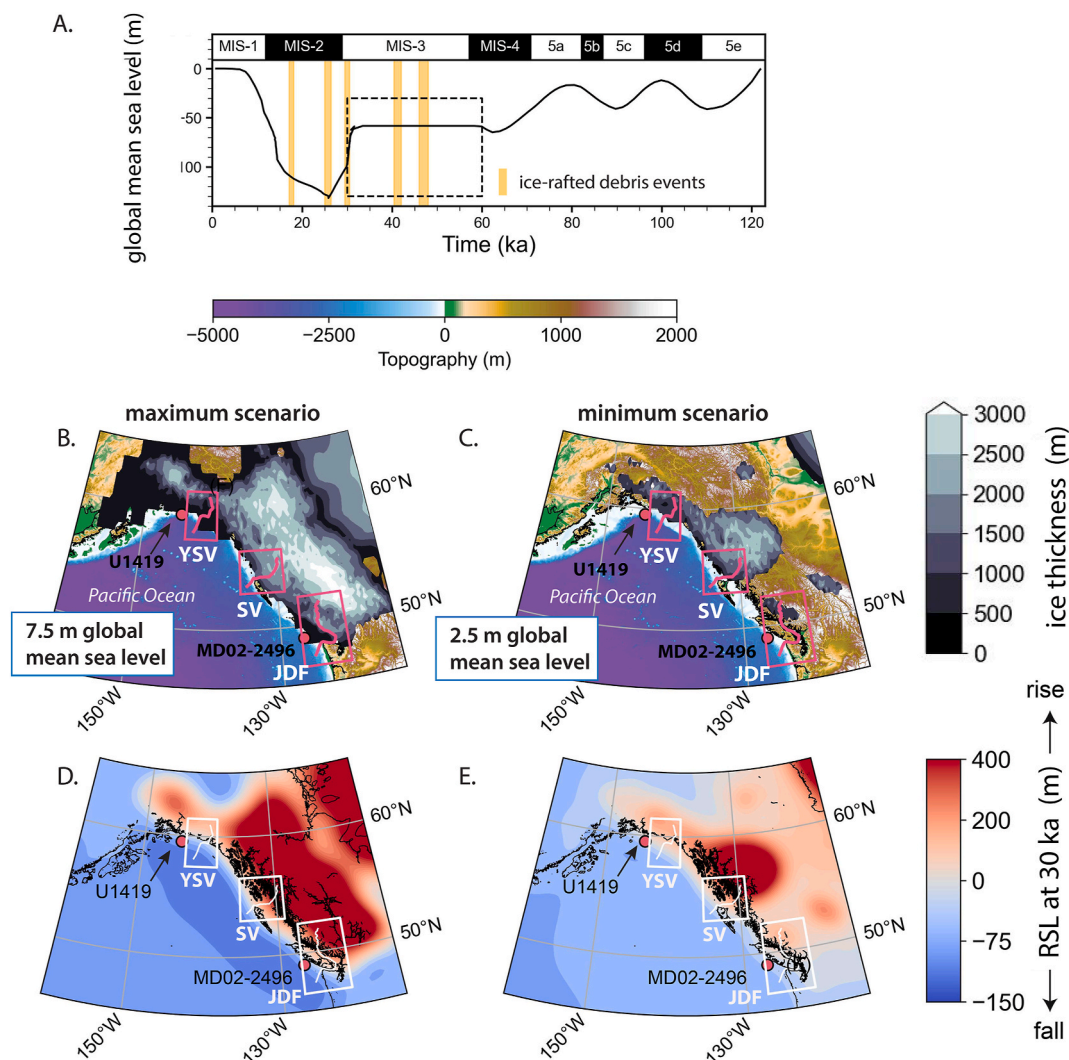

Fig. 2. A. Global mean sea level history for both the minimum and maximum ice sheet scenario. Ice sheet thickness, held constant from 60 to 30 ka in the (B) maximum ice sheet scenario, and (C) minimum ice sheet scenario. Relative sea level (RSL) at 30 ka for (D) maximum ice sheet scenario and (E) minimum ice sheet scenario (blue; relative sea level lower or topography uplifted relative to today; red; relative sea level higher or topography subsided relative to today). (For interpretation of the references to colour in this figure legend, the reader is referred to the Web version of this article.)

viscosity of 1×10^{19} Pa s, a viscosity of 2×10^{20} Pa s for the remainder of the upper mantle, and 3×10^{21} Pa s for the lower mantle. Inferences of Earth structure are based on fitting GIA constraints in southeast Alaska (Marsman et al., 2021), southern British Columbia (Clague and James, 2002; James et al., 2009; Yousefi et al., 2018) or global or regional seismic tomography models (Clark et al., 2019; Pan et al., 2022), and these studies suggest a thin effective lithospheric thickness (30–70 km) and a low-viscosity asthenosphere representing between 140 and 380 km of the upper mantle, with viscosities ranging from 1×10^{19} Pa s to 1×10^{20} Pa s. We perform sensitivity tests by varying the values for lithospheric thickness, upper mantle viscosity, and lower mantle viscosity, and discuss the sensitivity of our results to our Earth model selection in Supplementary Material (Supplementary Figs. 1–5). Paleotopography is calculated by subtracting the computed spatial field of sea-level change from modern day topography.

2.2. Ice sheet history reconstruction

We constructed two end-members of idealized global ice sheet history that explore the uncertainty of plausible Cordilleran Ice Sheet size prior to the Last Glacial Maximum (spanning MIS 3, from 60 to 30 ka). The maximum scenario Cordilleran Ice Sheet end-member (Fig. 2A) contains an ice sheet volume of 7.5 equivalent global mean sea level (GMSL) from 60 to 30 ka (close to the estimated Last Glacial Maximum volume of 8–9 m GMSL; Seguinot et al., 2016) while the minimum scenario end-member contains an ice sheet volume of 2.5 m GMSL. The minimum scenario still meets the requirement for marine terminating ice near Yakutat Sea Valley, however it does not contain marine terminating ice near Juan de Fuca (Fig. 2B). These ice sheet histories are input to our glacial isostatic adjustment simulations predicting sea level change over the last glacial cycle (from 120 ka to 0 ka).

To construct these ice sheet histories, we modified the global ice sheet reconstruction ICE-PC. The ICE-PC ice history uses the deglacial ICE-6G (Peltier and Fairbanks, 2006) ice geometries to populate the global mean sea level curve in Pico et al. (2017), and makes the standard assumption that the ice sheet grows in the same geometry in which it melts. We modify the base ICE-PC ice sheet history to include more recent reconstructions of ice sheet geometries for the MIS 3 Cordilleran Ice Sheet. We adopt ice sheet thicknesses from the dynamic ice sheet model simulations performed in Seguinot et al. (2016) using the GRIP climate forcing, and identify the most extensive modeled Cordilleran Ice Sheet at 57 ka. We use this ice thickness reconstruction (GRIP in Seguinot et al., 2016) at 57 ka as our "maximum scenario". Because the domain of the dynamic ice sheet simulations did not include the Aleutian Islands sector of the Cordilleran Ice Sheet, we patch the Seguinot et al. (2016) ice thickness into the maximum Cordilleran Ice Sheet scenario reconstructed into the global base ICE-PC ice history at 62 ka. This ice sheet represents the maximum scenario in our idealized reconstruction, and is held constant from 60 to 30 ka (Fig. 2C).

We adopt the predicted ice thickness from the GRIP simulation in Seguinot et al. (2016) at 46 ka for the minimum Cordilleran scenario (also held constant from 60 to 30 ka); this simulated ice sheet represents the smallest scenario within the set of ice sheet simulations that is characterized by marine terminating ice near Yakutat Sea Valley (where a nearby sediment core contains evidence for ice rafted debris across this interval; U1419; Fig. 1). Although there is also evidence for ice rafted debris near the Juan de Fuca Strait, time steps of the GRIP simulation from Seguinot et al. (2016) that produce marine terminating ice near the Juan de Fuca Strait contain an ice volume very similar to the maximum scenario. Therefore, we chose an ice sheet distribution for the minimum scenario that only has marine terminating ice near Yakutat Sea Valley. In our results, we consider the role of GIA on the Juan de Fuca ice stream for the minimum scenario, even though the minimum scenario does not contain ice in the Juan de Fuca region. Nonetheless, we make this comparison to understand the impact of longer-term ice loading on the Juan de Fuca ice stream, as there may have been brief time intervals (<5

ky) when ice flowed through the Juan de Fuca ice stream within a longer time duration of minimal or no ice loading.

We also explore a "variable" ice history that uses the minimum scenario as a base, with cycles of ice sheet growth and decay (expanding and contracting between the minimum and maximum scenarios), that correspond to the timing of ice rafted debris events near both Juan de Fuca Strait and Yakutat Sea Valley at 48 ka, 40 ka, and 30 ka (yellow; Fig. 2A; Supplementary Fig. 6), thus satisfying the geologic record. We show that our results with this "variable" ice history, which vacillates between the minimum and maximum scenario during growth and melt cycles at the times of ice rafted debris events, are very similar to our results using the base minimum ice sheet scenario (Supplementary Fig. 7).

To simplify comparison across these reconstructions, we assigned each ice history the same global mean sea level history. This global mean sea level history is identical to ICE-PC (Pico, Creveling and Mitrovica, 2017) except for the time interval from 60 ka to 30 ka, where global mean sea level is held constant at -70 m (Fig. 2A). To keep global mean sea level consistent across all ice sheet reconstructions, we calculate the difference in ice volume between the maximum scenario and the minimum and variable scenario, and assign the excess ice volume to the Antarctic Ice Sheet, sufficiently far that this does not impact our GIA predictions near the Cordilleran Ice Sheet (Supplementary Material). While global mean sea level was almost certainly not constant across MIS 3 (Siddall et al., 2008), maintaining global mean sea level the same across all of our ice sheet reconstructions allows us to compare the impact of Cordilleran Ice Sheet loads on predicted GIA patterns, and ultimately isolate the effect of GIA on our predicted grounding line persistence zones. Our approach targets the longer-wavelength scale of continental ice sheet loading, rather than transient smaller-scale GIA patterns in response to local loading changes as ice streams advance or retreat (Gomez et al., 2010). Given uncertainty on Cordilleran Ice Sheet size, which could range between our maximum and minimum scenario, a simplified end-member set of ice sheet reconstructions permits us to capture a range of possible GIA magnitudes and patterns.

2.3. Reconstructing ice stream paleotopography

We identified 3 major marine terminating ice streams that drained the Cordilleran Ice Sheet into the Pacific Ocean (magenta; Fig. 1). To reconstruct the paleo-elevation profiles beneath these ice streams across MIS 3, we first corrected modern topography (GEBCO; 15 arc seconds) for GIA at every time step. We then extracted the paleo-elevations underlying these ice streams by following submarine troughs, which align with documented flow pathways (Eyles et al., 2018; magenta; Fig. 1). Sedimentation and erosion likely changed the topography underlying these ice streams since MIS 3, with evidence suggesting that some of these ice streams are located in extremely high sedimentation environments (Gulick et al., 2015; Cowan et al., 2020). Although such high sedimentation rates (~ 1 m/ky since the LGM; Cosma and Hendy, 2008; Walczak, 2020a,b) would likely substantially change topography, we ignore topographic change due to sediment accumulation or erosion, focusing only on the impact of glacial isostatic adjustment. While information exists about sedimentation rates over this time period, it is challenging to reconstruct the paleoelevation of ice stream transects with confidence, given unknowns on the local history of glacial erosion and deposition for each ice stream. Therefore, sedimentation changes represent an uncertainty difficult to constrain in our topographic reconstructions and interpreted grounding line persistence zones.

2.4. Identifying potential grounding line persistence zones

We predict potential zones of grounding line persistence for each ice stream by extracting its topographic profile (modern and 30 ka paleo-topography) and test for linear stability at 1 km-spaced nodes with a simple model representing a migration of the grounding line of a marine-

terminating ice stream (Equation (1); Robel et al., 2018) for 100 different combinations of surface mass balance (0.1–0.3 $\frac{m}{yr}$) and basal friction (1.620e6–6.620e6 $Pa \cdot \frac{m}{s}$) values at each node (Skeena Valley ~425 nodes, Yakutat Sea Valley ~275, Juan de Fuca Strait ~425 nodes):

$$h_g \frac{dL}{dt} = PL - \Omega h_g^\beta \tag{1}$$

where,

$$\beta = \frac{m + n + 3}{m + 1} \tag{2}$$

$$\Omega = \frac{A(\rho_i g)^{n+1} \left(1 - \frac{\rho_i}{\rho_w}\right)^n}{(4^n C)^{\frac{1}{m+1}}} \tag{3}$$

$$h_g = h \frac{\rho_w}{\rho_i} \tag{4}$$

Where P is the upstream averaged surface mass balance (0.1–0.3 $\frac{m}{yr}$), L is the distance downstream from the ice divide, h_g is ice thickness at the grounding line, h is elevation at the grounding line, C is a basal friction coefficient (1.620e6–6.620e6 $Pa \cdot \frac{m}{s}$). We do not include ice shelf buttressing as an ice shelf is considered unlikely to have formed (Taylor et al., 2014). A node is considered to be a potential location of persistence if the ice flux into the node is equal to ice flux out (i.e., the location represents a fixed point (time derivative is zero) of Equation (1)) and the derivative of Equation (1) with respect to L is negative (i.e., the linear stability of the fixed point is negative)

$$Ph_g^{-1} + \left[PLh_g^{-2} + (\beta - 1)\Omega h_g^{\beta-1} \right] \frac{\rho_w}{\rho_i} \frac{dh}{dL} < 0. \tag{5}$$

This linear stability analysis of locations along the ice stream topographic profile assesses whether perturbations to the grounding line position return the grounding line to its original position. Since all other parameter are kept constant in space for simplicity, this linear stability analysis effectively determines where the bed topography is sufficiently prograde (deepening towards the ocean) to prevent runaway grounding line retreat. Values for parameters used in Equations (1)–(3) are found in Table 1.

For each ice stream topography profile, our analysis of the ensemble predicts a distribution of potential grounding line positions for different combinations of surface mass balance, and basal friction (Table 1), which we can compare between the maximum and minimum ice sheet histories, isolating the role of GIA in grounding line persistence. The simplicity of this model enables such a formal linear stability analysis over a wide range of different parameters. In reality, grounding line stability and migration are complex functions of many different glaciological and climatological processes which vary in time and space. Using a more complex glacier model would be necessary to access

transient grounding line behavior, but such an analysis would be computationally challenging over the wide range of parametric uncertainty inherent in paleoglaciological settings. Thus, we opt for this more idealized analysis to understand broad trends in potential grounding line behavior over MIS 3.

3. Results

3.1. Predicted glacial isostatic adjustment and ice stream paleo topography

We predicted relative sea-level change due to GIA using the two end-member ice sheet histories that represent the maximum and minimum Cordilleran Ice Sheet scenario from 60 to 30 ka (Fig. 2A–C). For the minimum scenario, at 30 ka (the end of MIS 3 and timing of Siku event #3), relative sea level across the marine terminating northern and central sectors of the Cordilleran Ice Sheet is at most 100 m higher (subsided relative to today; light pink; Fig. 2E), whereas the marine terminating southern sector is at most 50 m lower (uplifted relative to today; light blue; Fig. 2E). This broad pattern of sea level rise across most of the marine sector is caused by regional subsidence near the minimum scenario Cordilleran Ice Sheet. In contrast, in the maximum scenario, the marine sectors are dominated by sea level fall (uplifted relative to today) by up to 150 m (blue; Fig. 2D). Because Cordilleran Ice Sheet thickness is greater in the maximum scenario, the peripheral bulge along the Pacific coast of Canada and Alaska is more uplifted. In addition, the maximum scenario ice sheet spans the Aleutian Islands, and the loading in this region causes additional uplift to the south. The conjunction of these uplifted peripheral bulge regions, surrounding ice loading in the maximum scenario, causes sea level to fall (topography uplifted relative to today) along the marine terminating sectors of the Cordilleran Ice Sheet.

Relative sea level change from 60 to 30 ka across the transect of each ice stream is shown in Fig. 3. At the Yakutat Sea Valley terminus, relative sea level falls (topography uplifts) in the maximum scenario by < 50 m from 60 to 30 ka (Fig. 3A), whereas in the minimum scenario, relative sea level rises (topography subsides) by 50 m over this time (Fig. 3B). For the Skeena Valley ice stream terminus, relative sea level falls (topography uplifts) by < 50 m from 60 to 30 ka for the maximum scenario (Fig. 3C) and rises (topography subsides) by 50 m for the minimum scenario (Fig. 3D), while the upstream regions experience a relative sea level rise (topography subsided) by > 300 m for both scenarios (Fig. 3C/D). For the Juan de Fuca ice stream terminus, in the minimum scenario, relative sea level rises (topography subsides) by 50 m from 60 to 30 ka, whereas in the maximum scenario relative sea level falls (topography uplifts) by < 50 m in the downstream reaches and rises (topography subsides) by 200 m in the upstream reaches over this time (Fig. 3E/F).

The Yakutat Sea Valley ice stream maximum scenario paleotopography is uplifted by 50–100 m throughout the entire transect relative to the minimum scenario paleotopography (YSV; Fig. 4B; Fig. 5A). At 30 ka, the Skeena Valley ice stream maximum scenario paleotopography is uplifted by ~20 m in the downstream regions, and subsided by ~100 m in the upstream regions relative to the minimum scenario paleotopography (Fig. 4C; Fig. 5B). The Juan de Fuca ice stream maximum scenario paleotopography is uplifted by ~40 m in the downstream regions and >300 m in the upstream regions relative to the minimum scenario paleotopography (Fig. 4D; Fig. 5C).

3.2. Predicted grounding line persistence zones

We identified the grounding line persistence zones using the reconstructed paleotopography profiles corrected for GIA by performing a suite of 100 linear stability analyses at each node, which span a range of glaciological conditions (surface mass balance values and basal friction coefficient; Table 1). We consider the possible locations of grounding

Table 1
Parameters and values used for simulating grounding line persistence zones.

| Parameter	Description	Value
L	Distance downstream from ice divide	–
P	Upstream average surface mass balance (m/yr)	0.01-0.3
h_g	Ice thickness at the grounding line (m)	–
h	Topographic elevation at the grounding line (m)	–
A	Nye-Glen law coefficient ($Pa \cdot m^{-\frac{1}{n}} \cdot s^{-1}$)	2×10^{-24}
m	Weertman friction law exponent	1/3
n	Nye-Glen law exponent	3
C	Basal friction coefficient ($Pa \cdot m^{-\frac{1}{n}} \cdot s^{1/n}$)	$1.62\text{-}6.62 \times 10^6$
ρ_i	Ice density (kg/m³)	917
ρ_w	Sea water density (kg/m³)	1028
g	Gravitational acceleration (m/s²)	9.81
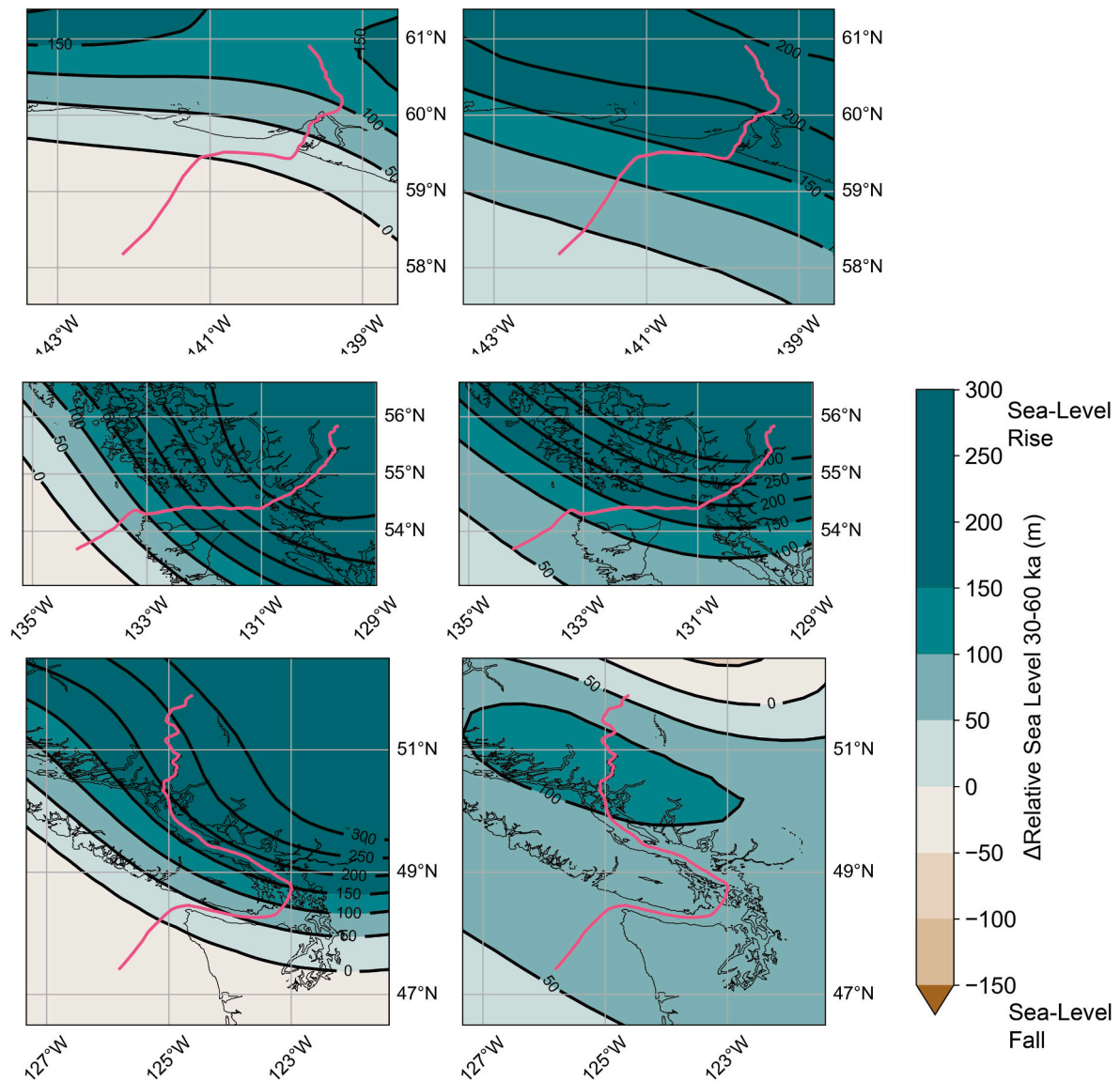
Fig. 3. Change in relative sea level from 60 to 30 ka ($RSL_{30 ka}$ – RSL_{60ka}) at each ice stream for the maximum ice sheet scenario (left) and the minimum ice sheet scenario (right) for (A/B) Yakutat Sea Valley (YSV), (C/D) Skeena Valley (SV), and (E/F) Juan de Fuca (JDF).

line persistence for each ice history at 30 ka. Fig. 5 shows the predicted grounding line persistence positions for paleotopography profiles corrected for GIA using the maximum scenario (red) and the minimum scenario (blue). For the minimum scenario paleotopography, multiple grounding line persistence zones span the ice stream transect for all three ice streams (Fig. 5). In contrast, for the maximum scenario paleotopography, the grounding line persistence zones are mostly restricted to either the shelf break or the steep slope at the modern coastline (Fig. 5). For all three ice streams, there is a higher likelihood for persistent grounding line zones along the mid-shelf region (or the central sectors of the Salish Sea, in the case of Juan de Fuca) in the minimum scenario. Although these three ice streams experience similar trends, the cause for grounding line persistence zone migration is different in each case, as each ice stream experiences a distinct pattern of GIA-induced topographic change. For the Skeena Valley ice stream (central Cordilleran), the maximum ice sheet scenario results in a GIA-corrected MIS 3 paleotopography where grounding line persistence zones are restricted to the shelf break and the modern coastline. In the maximum scenario, uplift of the Cordilleran Ice Sheet peripheral bulge in the downstream reaches (blue; Fig. 2E; purple; Fig. 4D) slightly increases the likelihood of persistent grounding lines downstream near the shelf break, whereas

subsidence due to ice loading in the central marine sector north of Haida Gwaii (red; Fig. 2E; green; Fig. 4D) decreases the likelihood of persistent grounding lines in the central sector of the shelf (100–300 km downstream; Fig. 5B). The maximum ice sheet scenario increases potential for steady-state grounding line positions near the shelf break for Skeena Valley by shallowing this section and reducing ice flux through the grounding line, whereas subsidence in the central sector of the shelf decreases stability by increasing ice flux and causing a negative mass balance. In the minimum ice sheet scenario, the higher elevation of the paleotopography, relative to the maximum scenario paleotopography, decreases ice flux through the grounding line at Skeena Valley, which permits more persistent grounding line zones in the central sector of the shelf (100–300 km downstream; Fig. 5B).

The Yakutat Sea Valley ice stream similarly has grounding line persistence zones shift away from the central section of the shelf with the maximum scenario (Fig. 4A), albeit due to a different GIA pattern. In this case, for the maximum ice sheet scenario, the entire marine sector of the ice stream is uplifted (blue; Fig. 3A; purple; Fig. 4B), shallowing the transect sufficiently to reduce flux through the grounding line, resulting in a positive mass balance over the entire transect, up until the shelf break where there are zones of potential grounding line persistence. The
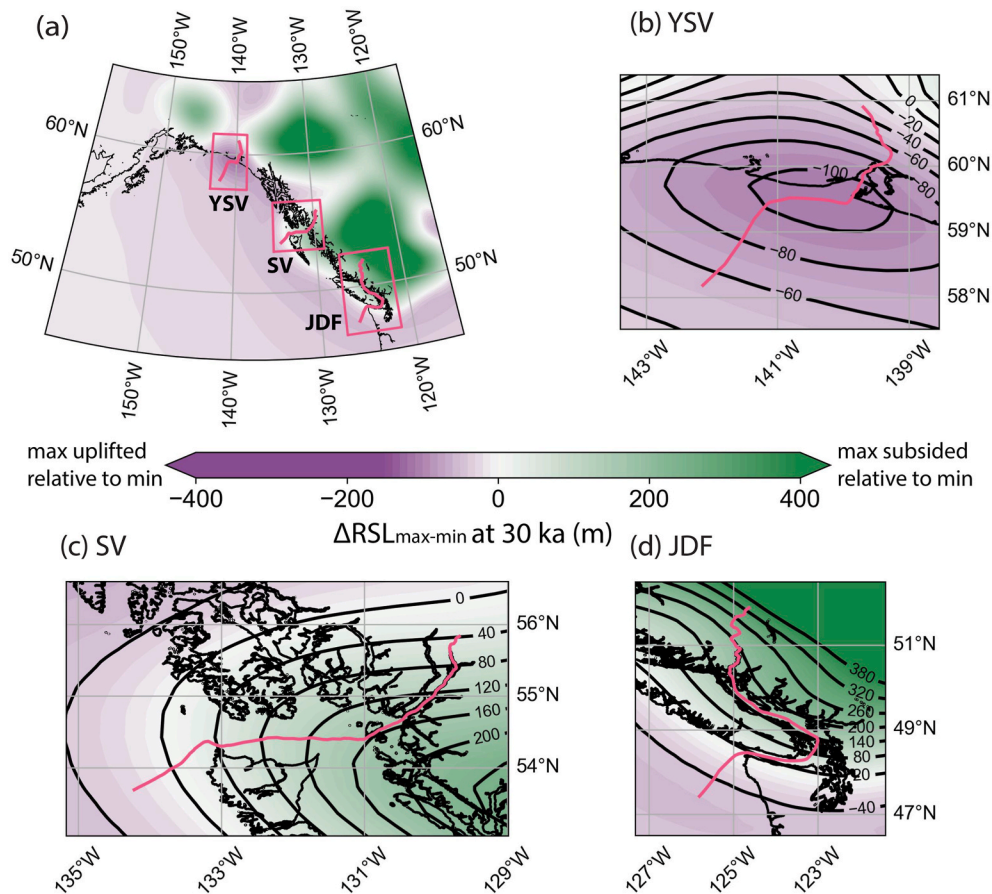
Fig. 4. A. Difference between maximum and minimum ice sheet scenario relative sea level at 30 ka (maximum - minimum) for (B) Yakutat Sea Valley (YSV), (C) Skeena Valley (SV), and (D) Juan de Fuca (JDF) ice streams.

minimum scenario for the Yakutat Sea Valley produces a smaller peripheral bulge, which causes a smaller sea level fall (smaller topographic uplift; Fig. 3B), resulting in a larger flux through the grounding line compared to the maximum scenario, and therefore more persistent grounding line zones along the central section of the shelf (100–300 km downstream; Fig. 5A).

For the Juan de Fuca ice stream, the GIA-corrected paleoelevation is similar in the downstream reaches between the two end-member ice sheet scenarios (Fig. 5C). However, the central sector (Salish Sea) is subsided in the maximum scenario relative to the minimum scenario (green; Fig. 4D), resulting in less persistent grounding line zones along the central sector for the maximum scenario (250–400 km downstream; Fig. 5C). In the minimum ice sheet scenario, the higher elevation of the paleotopography, relative to the maximum scenario paleotopography, decreases ice flux through the grounding line, which permits more persistent grounding line zones in the central sector of the Juan de Fuca ice stream in the Salish Sea (250–400 km downstream; Fig. 5C).

The contemporary coastline can be considered a potential zone of grounding line persistence, since the ice stream would become land terminating when it reaches this point. For all of these ice streams, the MIS 3 coastline is further inland than the modern coastline, as relative sea level is predicted to be higher at 30 ka along the modern coastline for both of the minimum and maximum scenario (pink and red; Fig. 2D/E). Therefore, the region beyond the MIS 3 coastline (higher than the elevations considered in Fig. 5) will be a zone of grounding line persistence.

4. Discussion

4.1. Impact of GIA on sensitivity to climate forcing

We found that, for the three ice streams considered here, glacial isostatic adjustment shifts the potential locations of persistent grounding lines away from the central sector of the shelf when the Cordilleran Ice Sheet is large across MIS 3 (maximum scenario; Fig. 5). Nevertheless, the influence of glacial isostatic adjustment on potential grounding line persistence zones will depend the ice stream path with respect to the predicted spatial pattern of topographic change.

Our results suggest that the loading history of the Cordilleran Ice Sheet during MIS 3 can determine the potential locations of persistent grounding lines within the ice sheet's marine sector. Through glacial isostatic adjustment, the history of the Cordilleran Ice Sheet can modulate how far an ice stream retreats, if triggered by an external forcing. For example, if the Cordilleran Ice Sheet were large across MIS 3, the Yakutat Sea Valley and Skeena Valley ice streams would respond differently to the same external forcing. The Skeena Valley is isostatically depressed when the Cordilleran Ice Sheet is large, which increases grounding line flux at any given location along the ice stream and creates a retrograde topography, exacerbating the potential for the marine ice sheet instability to occur (Fig. 5B). A small external forcing would be more likely to lead to a large retreat in grounding line location (Fig. 6). In contrast, GIA uplifts the Yakutat Sea Valley when the Cordilleran Ice Sheet is large, which decreases flux through the grounding line, leading to a positive mass balance. As a result, this marine-terminating ice stream will be less sensitive to external perturbations that cause grounding line retreat due to GIA shoaling grounding line depths when the Cordilleran Ice Sheet is large. Thus, a larger external perturbation
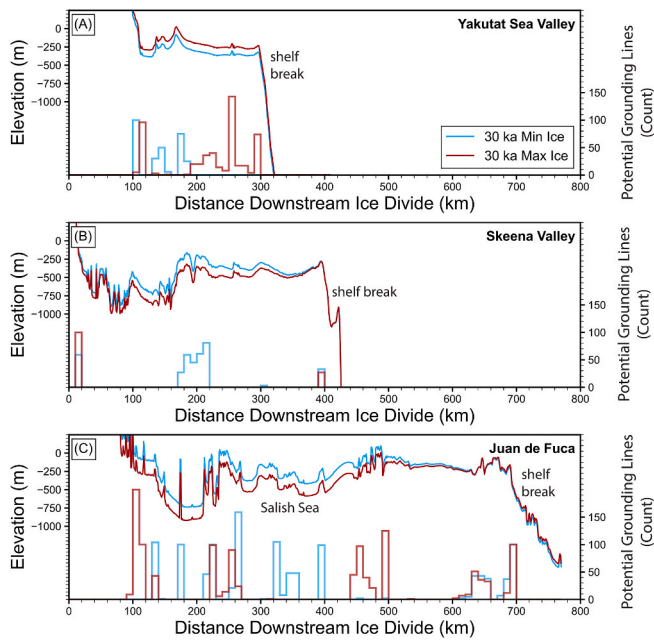
Fig. 5. Reconstructed paleotopography corrected for glacial isostatic adjustment with the maximum ice sheet scenario (red) and the minimum ice sheet scenario (blue), along with a histogram of the predicted potential persistent grounding line positions, for each ice stream: (A) Yakutat Sea Valley, (B) Skeena Valley, and (C) Juan de Fuca Strait. (For interpretation of the references to colour in this figure legend, the reader is referred to the Web version of this article.)
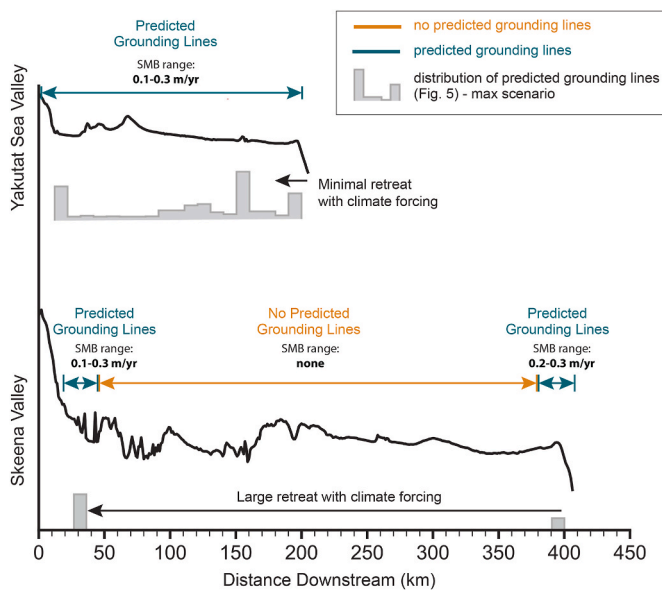

Fig. 6. Sensitivity of predicted grounding lines to climate forcing for the maximum ice sheet scenario for Yakutat Sea Valley (top) and Skeena Valley (bottom). Range of surface mass balance (SMB) values for zones with predicted grounding lines (blue) and no predicted grounding lines (orange). Black line shows present day topographic profile and gray histograms show distribution of predicted grounding lines in Fig. 5. (For interpretation of the references to colour in this figure legend, the reader is referred to the Web version of this article.)

climate forcings, we consider the range of accumulation rates allowed for grounding line zones to be persistent. For the Skeena Valley ice stream, persistent grounding line positions located near the edge of the continental shelf exist over a similar range of average upstream surface mass balance values for both ice sheet scenarios (minimum scenario: 0.19–0.3 m/yr; maximum scenario: 0.21–0.3 m/yr; Supplementary Fig. 8B). Therefore, grounding line retreat from the edge of the continental shelf in both scenarios would likely result from climate forcings equivalent to decreasing average upstream surface mass balance to below 0.19 m/yr. However, the central sector of the continental shelf (~200 km downstream; Fig. 5B) is ~140 m more subsided in the maximum ice sheet scenario compared to the minimum ice sheet scenario (green; Fig. 4C). This subsidence results in no potential grounding line steady-states ~200 km downstream in the maximum scenario (Fig. 5B), but steady-state grounding line positions for the minimum ice sheet scenario for the entire range of average upstream surface mass balance values (0.1–0.3 m/yr; Supplementary Fig. 8B). Therefore, in the minimum ice sheet scenario, if a climate forcing caused retreat of the Skeena Valley ice stream from the edge of the continental shelf, the ice stream might persist within the middle of the continental shelf, while, in the maximum ice sheet scenario, it would retreat further until the modern coastline.

We next consider the difference in surface mass balance values that result in persistent grounding line positions between the Yakutat Sea Valley and the Skeena Valley ice streams for the maximum ice scenario. Although both ice streams have persistent grounding line zones limited to the continental shelf edge and the modern coastline for the maximum ice scenario, the surface mass balance values associated with these persistent grounding line zones vary. Yakutat Sea Valley has persistent grounding line positions at the edge of the continental shelf for all values of average upstream surface mass balance (0.1–0.3 m/yr; Fig. 6; Supplementary Fig. 8A), while Skeena Valley has persistent grounding line positions for only larger average upstream surface mass balance values (0.21–0.3 m/yr; Fig. 6; Supplementary Fig. 8B). Therefore, a climate forcing equivalent to decreasing upstream average surface mass to below 0.2 m/yr would cause a negative mass balance which could lead the Skeena Valley grounding line position to substantially retreat to the modern coastline, due to its isostatically depressed, retrograde profile, while the Yakutat Sea Valley ice stream would remain at the continental shelf edge (Fig. 6).

4.2. Uncertainties on reconstructed paleotopography

Another important control on our predicted persistent grounding line zones is the antecedent topography, which determines the locations of topographic highs that serve as pinning points. Sedimentation and erosion have likely changed topography in this region since MIS 3, especially in sites like the Yakutat Sea Valley and Juan de Fuca, where there is evidence for extremely high sedimentation rates (~1 m/ky over the last deglaciation; Cosma and Hendy, 2008; Walczak, 2020a,b). Furthermore, over multiple glacial cycles, ice streams would have carved the valleys that serve as our transects. The history of sedimentation is an important uncertainty in our predictions, and our results may be different for topography associated with early glacial cycles, characterized by shallower valleys, not yet carved by glaciers.

Because the size of the Cordilleran Ice Sheet is not well constrained over most of MIS 3, we cannot determine which of the scenarios tested in this study is more likely. The end-member ice sheet scenarios we tested provide a plausible range of GIA magnitudes, and our linear stability analysis shows how these would impact the potential zones where grounding lines persist. To consider how GIA would change with a dynamic ice sheet that fluctuated between the maximum and minimum scenario, we created an additional "variable" ice history modifying the minimum scenario, where the ice sheet grows and melts suddenly at times when ice rafted debris events are recorded at 48 ka, 40 ka, and 30 ka. We found that this "variable" ice history produced potential

would be required for the Yakutat Sea Valley to retreat as far as the Skeena Valley would retreat under the same forcing (Fig. 6). Therefore, GIA can play a role in an ice stream's sensitivity to external forcings.

To explore how GIA modulates ice stream sensitivity to external

grounding line persistence zones similar to those predicted using the ice history with the minimum scenario (Supplementary Fig. 7).

We next explored the impact of our choice of Earth model on our predicted persistent grounding line zones. We predicted persistent grounding line zones between the two end-member ice histories using a set of alternate Earth models that vary lithospheric thickness and upper and lower mantle viscosity (Supplementary Material; Supplementary Figs. 1–5). We found that our results are sensitive to our choice of lithospheric thickness. In particular, predictions with a greater effective lithospheric thickness (96 km compared with 50 km in the main text), change our results showing that grounding line persistence zones shift from the continental shelf break and the modern coastline to the central sector of the ice stream, for both the Yakutat Sea Valley and Skeena Valley ice streams. For the Juan de Fuca ice stream, results are similar to the main text. In the case with an Earth model characterized with a greater effective lithospheric thickness (96 km), we predict similar persistent grounding line positions for the Yakutat Sea Valley ice stream in both the maximum and minimum scenario, whereas for Skeena Valley persistent grounding line zones are limited to only the modern coastline in the maximum scenario (Supplementary Fig. 1; Supplementary Fig. 4). The uplifted region of the peripheral bulge is further offshore in glacial isostatic adjustment predictions with a greater lithospheric thickness, causing smaller differences between the maximum and minimum scenario along the Skeena and Yakutat Sea Valley ice stream transects (Supplementary Fig. 1). Nevertheless, it is unlikely that an Earth model with a greater lithospheric thickness is realistic for this region. Inferences of lithospheric thickness and mantle viscosity suggests that this region is characterized by a relatively thin effective lithosphere (30–70 km) (Yousefi et al., 2018; Clark et al., 2019; Marsman et al., 2021; Pan et al., 2022). This region is located in a complex tectonic setting, dominated by the Cascadia subduction zone, and such settings are associated with a thinner effective lithospheric thickness (James et al., 2009). Therefore, while our results are sensitive to our choice of lithospheric thickness, we consider predictions with a thinner effective lithosphere more realistic and representative of topographic changes due to glacial isostatic adjustment for the Cordilleran Ice Sheet. Accurate predictions of topographic change due to glacial isostatic adjustment at each of these ice streams will require improved knowledge of both ice sheet history and 3D Earth structure, as incorporating lateral variations in lithospheric thickness and mantle viscosity across the Pacific coast can influence relative sea level (Clark et al., 2019; Marsman et al., 2021; Thompson et al., 2023).

4.3. MIS 3 Cordilleran Ice Sheet and global ice volumes

The timing of ice rafted debris events in the Pacific implies a dynamic Cordilleran Ice Sheet during MIS 3, which, in addition to being forced by climate changes in the ocean or the atmosphere, may be influenced by glacial isostatic adjustment-induced topographic change. Improved constraints on the extent and thickness of the Cordilleran Ice Sheet across the buildup phase will elucidate the extent to which glacial isostatic adjustment contributed to controlling the location of grounding lines. Moreover, the existence of ice rafted debris records is evidence of marine terminating ice streams that produce icebergs during MIS 3, and not all Cordilleran Ice Sheet reconstructions across MIS 3 incorporate marine sectors at the times of ice rafted debris events. This simple observation could improve ice sheet reconstructions by requiring marine terminating ice at least during ice rafted debris events.

Geologic data on land and in ocean sedimentary records may help determine which of our end-member ice sheet scenarios is most likely over the majority of MIS 3. Dating of bones within a cave setting in Southeastern Alaska from 45 ka to 20 ka show that at least part of the central coastal sector of the Cordilleran Ice Sheet (near Skeena Valley) was ice free over this interval, precluding the Cordilleran Ice Sheet from reaching maximum extent in this region over this time (Lesnek et al., 2018). Similarly, non-glacial deposits dated to ~45 to 30 ka (the

Olympia Interstadial) in both the Salish Sea and off the coast of Vancouver Island are evidence that the Juan de Fuca ice stream did not exist over this time (Hebda et al., 2016). Evidence for warm sea surface temperatures (5 °C) across the Last Glacial Maximum, along with inferences of a wet-based Cordilleran Ice Sheet (Clague and James, 2002), has been used to argue that Cordilleran ice streams only reached their marine limit during punctuated episodes of expansion (Taylor et al., 2014).

The size of the MIS 3 Cordilleran Ice Sheet ties into broader debates around global ice volume prior to the LGM (Batchelor et al., 2019; Dalton et al., 2022a,b; Farmer et al., 2022; Pico, 2022). Estimates of minimum global ice volume during mid MIS 3 range from 10 to 60 m below modern global mean sea level (−10 to −60 m GMSL; Batchelor et al., 2019), and the contribution of the Cordilleran Ice Sheet to MIS 3 global ice volumes is unclear. At the LGM, the Cordilleran Ice Sheet is thought to contain 8–9 m of equivalent GMSL (Seguinot et al., 2016). Reconstructions based on Seguinot et al. (2016) predict a Cordilleran Ice Sheet equivalent to 3.7–8.7 m GMSL in early MIS 3 at ~60 to 55 ka, and 1.5–2.8 m GMSL in mid-MIS 3 at ~45 to 40 ka. The smallest Cordilleran Ice Sheet reconstruction (PALEOMIST) is restricted to mountain regions, and contains only 0.06 m GMSL (Gowan et al., 2021). Our end-member ice sheet scenarios incorporate a 7.5 m GMSL ice sheet for the maximum scenario and a 2.5 m GMSL ice sheet for the minimum scenario. Estimates of Scandinavian Ice Sheet size during mid MIS 3 range from 0.8 m GMSL (Gowan et al., 2021) to 10 m GMSL (Lambeck et al., 2006), with evidence for ice free conditions (Helmens and Engels, 2010; Wohlfarth, 2010) and even recent work suggesting the Eurasian ice sheet was fully deglaciated during mid-MIS 3 (Mangerud et al., 2023). Recent estimates of a smaller Laurentide Ice Sheet during MIS 3, with global mean sea level near −40 m, hold between 10 m GMSL (Gowan et al., 2021) and 16 m GMSL (Pico et al., 2017, 2018). Antarctic ice thickness during MIS 3 is not well constrained, although unglaciated coastlines in Prydz Bay (East Antarctica) have been used to argue for similar ice extent to today (Berg et al., 2010, 2016), while high relative sea level, close to modern, in the same Prydz Bay region has been used to argue for greater local ice loading at MIS 3, equivalent to 0.5 m GMSL (Berkman et al., 1998; Hodgson et al., 2009; Gao et al., 2020; Ishiwa et al., 2021). Furthermore, MIS 3 global ice volumes and Cordilleran Ice Sheet size has implications for the flooding history of the Bering Strait (Pico et., 2020; Farmer et al., 2022), which can modulate climate by connecting the Pacific and Arctic oceans (Hu et al., 2012; Praetorius et al., 2020, 2023). Improving estimates of Cordilleran Ice Sheet size, for example, by finding nearby relative sea level records sensitive to this ice loading, will be important for quantifying the total contribution of individual ice sheets to global sea level across MIS 3.

5. Conclusion

Our study highlights the potential role of glacial isostatic adjustment in modulating where grounding lines may persist over the ice age. Depending on the size of the Cordilleran Ice Sheet in the period leading into the LGM, glacial isostatic adjustment could have acted to stabilize or destabilize marine-terminating grounding lines across the Pacific shelf. Glacial isostatic adjustment plays an important role in determining where grounding lines can persist, and changes the sensitivity of ice streams to climate forcing. Nevertheless, the extent to which glacial isostatic adjustment modulates persistent grounding line zones depends on the location of the ice stream with respect to sea level change patterns, in addition to the underlying bedrock topography. Refining the Cordilleran Ice Sheet history across the glacial buildup phase will allow us to disentangle the role of solid Earth feedbacks on grounding line dynamics for individual ice streams. Quantifying the role of glacial isostatic adjustment on marine ice sheet dynamics, in addition to understanding how the ice sheet would have responded to climate forcing, can elucidate the mechanisms causing the abrupt events, ranging from rapid ice discharge to megafloods, documented in the Pacific across the

last ice age.

CRediT authorship contribution statement

T.P contributed to conceptualization. A.R., T.P, and S.T.K contributed to methodology and software. S.T.K and C.V. contributed to formal analysis and investigation. S.T.K contributed to visualization. T.P wrote the original manuscript draft with review and editing input from all authors.

Declaration of competing interest

The authors declare that they have no known competing financial interests or personal relationships that could have appeared to influence the work reported in this paper.

Acknowledgments

Appendix A. Supplementary data

Supplementary data to this article can be found online at https://doi.org/10.1016/j.quascirev.2025.109427

Data availability

The data that support this study (ice histories and GIA output) are publicly available at https://doi.org/10.5281/zenodo.15535928

References

Adhikari, S., et al., 2014. Future Antarctic bed topography and its implications for ice sheet dynamics. Solid Earth 5 (1), 569–584. https://doi.org/10.5194/se-5-569-2014.

Alley, R.B., 1993. In search of ice-stream sticky spots. J. Glaciol. 39 (133), 447–454. https://doi.org/10.3189/S0022143000016336.

Barletta, V.R., et al., 2018. Observed rapid bedrock uplift in Amundsen Sea Embayment promotes ice-sheet stability. Science 360 (6395), 1335–1339. https://doi.org/10.1126/science.aao1447.

Bassis, J.N., Petersen, S.V., Cathles, L.M., 2017. Heinrich events triggered by ocean forcing and modulated by isostatic adjustment. Nature 5–7. https://doi.org/10.1038/nature21069.

Batchelor, C.L., et al., 2019. The configuration of Northern Hemisphere ice sheets through the Quaternary. Nat. Commun. 10 (1), 1–10. https://doi.org/10.1038/s41467-019-11601-2.

Berg, S., et al., 2010. No significant ice-sheet expansion beyond present ice margins during the past 4500 yr at Rauer Group, East Antarctica. Quat. Res. 74 (1), 23–25. https://doi.org/10.1016/j.yqres.2010.04.004.

Berg, S., et al., 2016. Unglaciated areas in East Antarctica during the last glacial (marine isotope stage 3) – new evidence from Rauer group. Quat. Sci. Rev. 153, 1–10. https://doi.org/10.1016/j.quascirev.2016.08.021.

Berkman, P.A., et al., 1998. Circum-Antarctic coastal environmental shifts during the Late Quaternary reflected by emerged marine deposits. Antarct. Sci. 10 (3), 345–362. https://doi.org/10.1017/S0954102098000406.

Booth, D.B., et al., 2003. The cordilleran ice sheet. Dev. Quat. Sci. 1 (C), 17–43. https://doi.org/10.1016/S1571-0866(03)01002-9.

Briner, J.P., Kaufman, D.S., 2008. Late Pleistocene mountain glaciation in Alaska: key chronologies. J. Quat. Sci. 23 (6–7), 659–670. https://doi.org/10.1002/jqs.1196.

Clague, J.J., et al., 2005. Early growth of the last Cordilleran ice sheet deduced from glacio-isostatic depression in southwest British Columbia, Canada. Quat. Res. 63 (1), 53–59. https://doi.org/10.1016/j.yqres.2004.09.007.

Clague, J.J., Hebda, R.J., Mathewes, R.W., 1990. Stratigraphy and paleoecology of pleistocene interstadial sediments, central British Columbia. Quat. Res. 34 (2), 208–226. https://doi.org/10.1016/0033-5894(90)90032-G.

Clague, J.J., James, T.S., 2002. History and isostatic effects of the last ice sheet in southern British Columbia British Columbia. Quat. Sci. Rev. 21, 70–87. https://doi.org/10.1016/S0277-3791(01)00070-1.

Clark, J., Mitrovica, J.X., Latychev, K., 2019. Glacial isostatic adjustment in central Cascadia : insights from three-dimensional Earth modeling. Geology 47 (4), 295–298.

Clark, P.U., et al., 2009. The last glacial maximum. Science (New York, N.Y.) 325 (5941), 710–714. https://doi.org/10.1126/science.1172873.

Cosma, T., Hendy, I.L., 2008. Pleistocene glacimarine sedimentation on the continental slope off Vancouver Island , British Columbia. Mar. Geol. 255, 45–54. https://doi.org/10.1016/j.margeo.2008.07.001.

Cowan, E.A., et al., 2020. Sediment controls dynamic behavior of a cordilleran ice stream at the last glacial maximum. Nat. Commun. https://doi.org/10.1038/s41467-020-15579-0 [Preprint].

Dalton, A.S., et al., 2019. Was the Laurentide ice sheet significantly reduced during marine isotope stage 3. Geology 47 (2), 111–114.

Dalton, A.S., et al., 2022a. The marine δ 18 O record overestimates continental ice volume during Marine Isotope Stage 3. Global Planet. Change 212 (April), 103814. https://doi.org/10.1016/j.gloplacha.2022.103814.

Dalton, A.S., Stokes, C.R., Batchelor, C.L., 2022b. Evolution of the Laurentide and innuitian ice sheets prior to the last glacial maximum (115 ka to 25 ka). Earth Sci. Rev. 224 (November 2021), 103875. https://doi.org/10.1016/j.earscirev.2021.103875.

Eyles, N., Moreno, L.A., Sookhan, S., 2018. Ice streams of the late Wisconsin cordilleran ice sheet in western north America. Quat. Sci. Rev. 179, 87–122. https://doi.org/10.1016/j.quascirev.2017.10.027.

Farmer, J.R., et al., 2022. The Bering Strait was flooded 10,000 years before the last glacial maximum. Proceedings of the National Academy of Sciences, pp. 1–7. https://doi.org/10.1073/pnas.

Favier, L., et al., 2016. Dynamic influence of pinning points on marine ice-sheet stability: a numerical study in Dronning Maud Land, East Antarctica. Cryosphere 10 (6), 2623–2635. https://doi.org/10.5194/tc-10-2623-2016.

Gao, Y., et al., 2020. Ice sheet changes and GIA-induced surface displacement of the larsemann hills during the last 50 kyr. J. Geophys. Res. Solid Earth 125 (10). https://doi.org/10.1029/2020JB020167.

de Gelder, G., et al., 2022. High interstadial sea levels over the past 420ka from the Huon Peninsula, Papua New Guinea. Commun. Earth Environ. https://doi.org/10.1038/s43247-022-00583-7 [Preprint].

Gomez, N., et al., 2010. Sea Level as a Stabilizing Factor for Marine-Ice-Sheet Grounding Lines, pp. 1–4. https://doi.org/10.1038/NGEO1012. November.

Gomez, N., et al., 2012. Evolution of a coupled marine ice sheet-sea level model: coupled ice sheet, sea level model. J. Geophys. Res.: Earth Surf. 117 (F1). https://doi.org/10.1029/2011JF002128 n/a-n/a.

Gowan, E.J., et al., 2021. A new global ice sheet reconstruction for the past 80000 years. Nat. Commun. 1–9. https://doi.org/10.1038/s41467-021-21469-w, 2021.

Gulick, S.P.S., et al., 2015. Mid-Pleistocene climate transition drives net mass loss from rapidly uplifting St . Elias Mountains , Alaska. Proc. Natl. Acad. Sci. USA. https://doi.org/10.1073/pnas.1512549112 [Preprint].

Hebda, R.J., Lian, O.B., Hicock, S.R., 2016. Olympia Interstadial: vegetation, landscape history, and paleoclimatic implications of a mid-Wisconsinan (MIS3) nonglacial sequence from southwest British Columbia, Canada. In: Fisher, T.G. (Ed.), Can. J. Earth Sci. 53 (3), 304–320. https://doi.org/10.1139/cjes-2015-0122.

Helmens, K., Engels, S., 2010. Ice-free conditions in eastern Fennoscandia during early Marine Isotope Stage 3 : lacustrine records, 2010(Ilvonen 1973). https://doi.org/10.1111/j.1502-3885.2010.00142.x.

Hendy, I.L., Cosma, T., 2008. Vulnerability of the Cordilleran Ice Sheet to iceberg calving during late Quaternary rapid climate change events: high-resolution North Pacific ird. Paleoceanography 23 (2). https://doi.org/10.1029/2008PA001606 n/a-n/a.

Hewitt, A.T., McDonald, B., Bornhold, B.D., 1997. Ice-rafted debris in the North Pacific and correlation to North Atlantic climatic events. Geophys. Res. Lett. 24 (24), 3261–3264. https://doi.org/10.1029/97GL03264.

Hodgson, D.A., et al., 2009. A geological constraint on relative sea level in marine isotope stage 3 in the Larsemann Hills, Lambert glacier region, East Antarctica (31 366–33 228calyrBP). Quat. Sci. Rev. 28 (25–26), 2689–2696. https://doi.org/10.1016/j.quascirev.2009.06.006.

Hu, A., et al., 2012. In: Role of the Bering Strait on the Hysteresis of the Ocean Conveyor Belt Circulation and Glacial Climate Stability, vol.109, pp. 6417–6422. https://doi.org/10.1073/pnas.1116014109, 17.

Ishiwa, T., Okuno, J., Suganuma, Y., 2021. Excess ice loads in the Indian Ocean sector of East Antarctica during the last glacial period. Geology XX (Xx), 1–5. https://doi.org/10.1130/G48830.1/5327672/g48830.pdf.

James, T.S., et al., 2009. Viscosity of the asthenosphere from glacial isostatic adjustment and subduction dynamics at the northern Cascadia subduction zone, British Columbia, Canada. J. Geophys. Res. Solid Earth 114 (4), 1–13. https://doi.org/10.1029/2008JB006077.

Johnston, P., 1993. The effect of spatially non-uniform water loads on prediction of sea-level change. Geophys. J. Int. 114 (3), 615–634.

Kaufman, D.S., et al., 2011. Alaska palaeo-glacier Atlas (Version 2). In: Developments in Quaternary Sciences. Elsevier, pp. 427–445. https://doi.org/10.1016/B978-0-444-53447-7.00033-7.

Kendall, R.A., Mitrovica, J.X., Milne, G.A., 2005. On post-glacial sea level - II. Numerical formulation and comparative results on spherically symmetric models. Geophys. J. Int. 161 (3), 679–706. https://doi.org/10.1111/j.1365-246X.2005.02553.x.

Kingslake, J., et al., 2018. Extensive retreat and re-advance of the west Antarctic ice sheet during the Holocene. Nature. https://doi.org/10.1038/s41586-018-0208-x [Preprint].

Kodama, S.T., et al., 2025. Impact of glacial isostatic adjustment on zones of potential grounding line stability in the Ross Sea Embayment (Antarctica) since the Last Glacial Maximum. https://doi.org/10.5194/egusphere-2024-3465.

Lambeck, K., et al., 2003. Water-load definition in the glacio-hydro-isostatic sea-level equation. Quat. Sci. Rev. 22 (2–4), 309–318. https://doi.org/10.1016/S0277-3791(02)00142-7.

Lambeck, K., et al., 2006. Constraints on the Late Saalian to early Middle Weichselian ice sheet of Eurasia from field data and rebound modelling. Boreas. https://doi.org/10.1080/03009480600781875 [Preprint].

Lesemann, J., 2013. A refined understanding of the paleoenvironmental history recorded at the Okanagan Centre section, an MIS 4 stratotype, south-central British Columbia, Canada. J. Quat. Sci. 28 (8), 729–747. https://doi.org/10.1002/jqs.2665.

Lesnek, A.J., et al., 2018. Deglaciation of the Pacific coastal corridor directly preceded the human colonization of the Americas. Sci. Adv. 4 (5), eaar5040. https://doi.org/10.1126/sciadv.aar5040.

Lisiecki, L.E., Raymo, M.E., 2005. A Pliocene-Pleistocene stack of 57 globally distributed benthic δ18O records. Paleoceanography 20 (1), 1–17. https://doi.org/10.1029/2004PA001071.

Maier, E., et al., 2018. North Pacific freshwater events linked to changes in glacial ocean circulation. Nature 559 (7713), 241–245. https://doi.org/10.1038/s41586-018-0276-y.

Mangerud, J., et al., 2023. Did the Eurasian ice sheets melt completely in early Marine Isotope Stage 3? New evidence from Norway and a synthesis for Eurasia. Quat. Sci. Rev. 311, 108136. https://doi.org/10.1016/j.quascirev.2023.108136.

Marsman, C.P., et al., 2021. The impact of a 3-D Earth structure on glacial isostatic adjustment in southeast Alaska following the little ice age journal of geophysical research : solid Earth. J. Geophys. Res. Solid Earth 1–17. https://doi.org/10.1029/2021JB022312, 2005.

Mathewes, R.W., et al., 2015. Early Wisconsinan (MIS 4) glaciation on Haida Gwaii, British Columbia, and implications for biological refugia. In: Fisher, T. (Ed.), Can. J. Earth Sci. 52 (11), 939–951. https://doi.org/10.1139/cjes-2015-0041.

McDonald, E.V., Sweeney, M.R., Busacca, A.J., 2012. Glacial outburst floods and loess sedimentation documented during oxygen isotope stage 4 on the Columbia plateau, Washington state. Quat. Sci. Rev. 45, 18–30. https://doi.org/10.1016/j.quascirev.2012.03.016.

McKenzie, M.A., et al., 2023. Differential impact of isolated topographic bumps on ice sheet flow and subglacial processes. Cryosphere 17 (6), 2477–2486. https://doi.org/10.5194/tc-17-2477-2023.

Milne, G.A., Mitrovica, J.X., 1996. Postglacial sea-level change on a rotating Earth: first results from a gravitationally self-consistent sea-level equation. Geophys. J. Int. 126 (3), F13–F20. https://doi.org/10.1111/j.1365-246X.1996.tb04691.x.

Milne, G.A., Mitrovica, J.X., Davis, J.L., 1999. Near-field hydro-isostasy: the implementation of a revised sea-level equation. Geophys. J. Int. 139, 464–482. https://doi.org/10.1046/j.1365-246x.1999.00971.x.

Pan, L., et al., 2022. The influence of lateral Earth structure on inferences of global ice volume during the Last Glacial Maximum. Quat. Sci. Rev. 290, 107644. https://doi.org/10.1016/j.quascirev.2022.107644.

Peltier, W.R., Fairbanks, R.G., 2006. Global glacial ice volume and Last Glacial Maximum duration from an extended Barbados sea level record. Quat. Sci. Rev. 25, 3322–3337. https://doi.org/10.1016/j.quascirev.2006.04.010.

Pico, T., et al., 2016. Global ice volume during MIS 3 inferred from a sea-level analysis of sedimentary core records in the Yellow River Delta. Quat. Sci. Rev. 152, 72–79. https://doi.org/10.1016/j.quascirev.2016.09.012.

Pico, T., et al., 2018. Refining the Laurentide Ice Sheet at Marine Isotope Stage 3 : a data-based approach combining glacial isostatic simulations with a dynamic ice model. Quat. Sci. Rev. 195, 171–179. https://doi.org/10.1016/j.quascirev.2018.07.023.

Pico, T., et al., 2019. Leveraging the rapid retreat of the Amundsen Gulf ice stream 13 , 000 Years Ago to Reveal insight into North American deglaciation. Geophys. Res. Lett. 1–7. https://doi.org/10.1029/2019GL084789.

Pico, T., 2022. Toward new and independent constraints on global mean seasea-level highstands during the last glaciation (marine isotope stage 3, 5a, and 5c). Paleoceanogr. Paleoclimatol. 1–4. https://doi.org/10.1029/2022PA004560.

Pico, T., Creveling, J.R., Mitrovica, J.X., 2017. Sea-Level records from the U.S. Mid-atlantic constrain Laurentide ice sheet extent during marine isotope stage 3. Nat. Commun. 8 (May), 15612. https://doi.org/10.1038/ncomms15612.

Pico, T., Mitrovica, J.X., Mix, A.C., 2020. Sea level fingerprinting of the Bering Strait flooding history detects the source of the Younger Dryas climate event. Sci. Adv. 6 (9). https://doi.org/10.1126/sciadv.aay2935.

Praetorius, S.K., et al., 2020. The role of Northeast Pacific meltwater events in deglacial climate change. Sci. Adv. 6 (February), 1–18. https://doi.org/10.1126/sciadv.aay2915.

Praetorius, S.K., et al., 2023. Ice and ocean constraints on early human migrations into North America along the Pacific coast. Proc. Natl. Acad. Sci. 120 (7), e2208738120. https://doi.org/10.1073/pnas.2208738120.

Robel, A.A., et al., 2022. Ambiguous stability of glaciers at bed peaks. J. Glaciol. 68 (272), 1177–1184. https://doi.org/10.1017/jog.2022.31.

Robel, Alexander A., Roe, G.H., Haseloff, M., 2018b. Response of marine-terminating glaciers to forcing: time scales, sensitivities, instabilities, and stochastic dynamics. J. Geophys. Res.: Earth Surf. 123 (9), 2205–2227. https://doi.org/10.1029/2018JF004709.

Robel, A.A., Tziperman, E., 2016. The role of ice stream dynamics in deglaciation. J. Geophys. Res.: Earth Surf. 121 (8), 1540–1554. https://doi.org/10.1002/2016JF003937.

Schoof, C., 2007. Ice sheet grounding line dynamics : steady states , stability , and hysteresis. J. Geophys. Res. 112 (July), 1–19. https://doi.org/10.1029/2006JF000664.

Schoof, C., 2012. Marine ice sheet stability. J. Fluid Mech. 698, 62–72. https://doi.org/10.1017/jfm.2012.43.

Seguinot, J., et al., 2016. Numerical simulations of the Cordilleran ice sheet through the last glacial cycle. Cryosphere 10 (2), 639–664. https://doi.org/10.5194/tc-10-639-2016.

Siddall, M., et al., 2008. Marine Isotope Stage 3 sea level fluctuations: data synthesis and new outlook. Rev. Geophys. 46, 1–29. https://doi.org/10.1029/2007RG000226.1, 2007.

Stokes, C.R., et al., 2015. On the reconstruction of palaeo-ice sheets : recent advances and future challenges. Quat. Sci. Rev. 125. https://doi.org/10.1016/j.quascirev.2015.07.016.

Stroeven, A.P., et al., 2010. Investigating the glacial history of the northern sector of the Cordilleran Ice Sheet with cosmogenic 10 Be concentrations in quartz. Quat. Sci. Rev. 29 (25–26), 3630–3643. https://doi.org/10.1016/j.quascirev.2010.07.010.

Stroeven, A.P., et al., 2014. Investigating absolute chronologies of glacial advances in the NW sector of the Cordilleran Ice Sheet with terrestrial in situ cosmogenic nuclides. Quat. Sci. Rev. 92, 429–443. https://doi.org/10.1016/j.quascirev.2013.09.026.

Taylor, M.A., Hendy, I.L., Pak, D.K., 2014. Deglacial ocean warming and marine margin retreat of the cordilleran ice sheet in the North Pacific ocean. Earth Planet Sci. Lett. 403, 89–98. https://doi.org/10.1016/j.epsl.2014.06.026.

Thompson, S.B., et al., 2023. Three-dimensional glacial isostatic adjustment modeling reconciles conflicting geographic trends in North American marine isotope stage 5a relative sea level observations. Geology [Preprint]. https://doi.org/10.1130/G51257.1.

Walczak, M.H., et al., 2020a. Phasing of millennial-scale climate variability in the pacific and Atlantic oceans. Science 7096 (October), 1–12.

Walczak, Maureen H., et al., 2020b. Phasing of millennial-scale climate variability in the Pacific and Atlantic oceans. Science 720 (November), 716–720.

Ward, B.C., Bond, J.D., Gosse, J.C., 2007. Evidence for a 55–50 ka (early Wisconsin) glaciation of the Cordilleran ice sheet, Yukon Territory, Canada. Quat. Res. 68 (1), 141–150. https://doi.org/10.1016/j.yqres.2007.04.002.

Whitehouse, P.L., et al., 2019. Solid Earth change and the evolution of the Antarctic ice sheet. Nat. Commun. 1–14. https://doi.org/10.1038/s41467-018-08068-y.

Wohlfarth, B., 2010. Ice-free Conditions in Sweden during Marine Oxygen Isotope Stage 3, vol. 39, pp. 377–398. https://doi.org/10.1111/j.1502-3885.2009.00137.x. Hemming 2004.

Yousefi, M., et al., 2018. Glacial isostatic adjustment along the Pacific coast of central North America. Quat. Sci. Rev. 193, 288–311. https://doi.org/10.1016/j.quascirev.2018.06.017.